Journal of Power Sources 253 (2014) 143–149

Contents lists available at ScienceDirect

Journal of Power Sources

journal homepage: www.elsevier.com/locate/jpowsour

Solvothermal synthesis of nano $LiMn_{0.9}Fe_{0.1}PO_4$: Reaction mechanism and electrochemical properties

Feipeng Ye [a,b], Li Wang [a,d,*], Xiangming He [a,c,*], Mou Fang [a,d], Zhongjia Dai [a,c], Jixian Wang [a], Chaochao Huang [a,d], Fang Lian [b], Jianlong Wang [a], Guangyu Tian [c], Minggao Ouyang [c]

[a] Institute of Nuclear and New Energy Technology, Tsinghua University, Beijing 100084, PR China
[b] School of Materials Science and Engineering, University of Science and Technology Beijing, Beijing 100083, PR China
[c] State Key Laboratory of Automotive Safety and Energy, Tsinghua University, Beijing 100084, PR China
[d] Huadong Institute of Lithium Ion Battery, Zhangjiagang, Jiangsu 215600, PR China

HIGHLIGHTS

- Feeding sequences is important in synthesis of LMFP through solvothermal.
- (010) face orientated LiMFP presents high electrochemical performance.
- A synthesis reaction mechanism of feeding sequence is proposed.
- The synthesized $LiMn_{0.9}Fe_{0.1}PO_4$ presents the discharge capacity of 150 mAh g^{-1}.

ARTICLE INFO

Article history:
Received 22 August 2013
Received in revised form
3 December 2013
Accepted 3 December 2013
Available online 12 December 2013

Keywords:
Feeding sequences
Solvothermal synthesis
Lithium manganese iron phosphate
Lithium ion battery

ABSTRACT

Solvothermal approach is used to synthesize $LiMn_{0.9}Fe_{0.1}PO_4$ (LMFP) nanomaterial for Li-ion batteries (LIBs). Experimental parameters such as feeding sequences, reaction time and reaction temperature are discussed and the obtained LMFP are characterized by XRD, SEM and TEM. To understand the formation of LMFP, a reaction mechanism is proposed. The proposed mechanism indicates that the suitable concentration of M_{Li} (M = Fe, Mn) antisite defect can improve the electrochemical performance of the material. The charge–discharge data of obtained LMFP shows that the $LiMn_{0.9}Fe_{0.1}PO_4$ material synthesized at 180 °C for 4 h and then sintering with sucrose at 650 °C for 5 h under argon protection has the highest discharge capacity, which is 149.2 mAh g^{-1} at 0.1C rate.

1. Introduction

Polyoxyanion cathode materials have been widely studied over the past 15 years [1–7], and the electrochemical properties of $LiFePO_4$ have improved significantly. Due to its high theoretical specific capacity, low cost, good electrochemical performance and chemical stability [8], $LiFePO_4$ has become a promising anode material.

For the reason of the theoretical energy density of $LiMnPO_4$ is 697 Wh kg^{-1}, much higher than 578 Wh kg^{-1} of $LiFePO_4$ [9], $LiMnPO_4$ become more and more popular recently [10,11]. However, its low electronic conductivity ($<10^{-10}$ S cm^{-1}) becomes one of the major obstructs of $LiMnPO_4$, which even lower than the $LiFePO_4$ (1.8×10^{-9} S cm^{-1}) [12,13]. Thereby, in order to make it as a promising candidate for future anode materials, one should focus on improving its conductive ability of both ions and electrons.

Approaches such as nanominiaturization, carbon-coating and doping are used to improve the conductive of $LiMnPO_4$. Nanominiaturization has the advantage of shortening the lithium ion migration distance. Other than solid-state reaction [14], more synthesis methods, such as sol–gel method [15], hydrothermal [16] and solvothermal methods [16,17] have been applied to nanominiaturize $LiMnPO_4$. Carbon-coating and cations (Fe, Co, Mg, Ti, Zr,

* Corresponding authors. Institute of Nuclear and New Energy Technology, Tsinghua University, Beijing 100084, PR China. Tel.: +86 10 89796073; fax: +86 10 89796031.
E-mail addresses: wang-l@tsinghua.edu.cn (L. Wang), hexm@tsinghua.edu.cn, hexiangming@tsinghua.org.cn (X. He).

0378-7753/$ – see front matter © 2013 Elsevier B.V. All rights reserved.
http://dx.doi.org/10.1016/j.jpowsour.2013.12.010

V, Fe, Gd and Zn) doping of $LiMnPO_4$ can improve its electrochemical performance [18]. It is reported that the carbon-coated $LiMn_{0.71}Fe_{0.29}PO_4$ can provide better electronic conductivity and has better electrochemical performance [19].

In this study, we report facile solvothermal processes that use two different feeding sequences to synthesis $LiMn_{0.9}Fe_{0.1}PO_4$. Reaction time and temperature are discussed as well. To investigate the reaction mechanism, we select the optimal solution feeding sequences (M + P + L) under the solvothermal condition of 180 °C for 12 h, and the reaction is monitored by apparent pH value and ICP analysis. To characterize the phase and morphology, the XRD, SEM and TEM are employed. The significant shift of infrared absorption can be used to detect the antisite defects. Finally, the synthesis condition is optimized to be at 180 °C with 4 h.

2. Experimental

2.1. Synthesis

All chemicals (AR grade) are purchased from Xilong Chemical Co., Ltd. The syntheses of $LiMn_{0.9}Fe_{0.1}PO_4$ by two different feeding sequences are prepared as follows: the first feeding sequence is S1 = L + P + M, by which the ethylene glycol solution of transition metal salts ($MnCl_2 \cdot H_2O$ and $FeSO_4 \cdot 7H_2O$) is slowly dripped into the ethylene glycol, $LiOH \cdot H_2O$ and H_3PO_4 mixture solution; The other feeding sequence is S2 = M + P + L, by which the ethylene glycol solution of $LiOH \cdot H_2O$ is slowly dripped into the ethylene glycol solution with mixture of H_3PO_4 and transition metal salts. The molar ratio of M^{2+}:$PO4^{3+}$:Li^+ is set at 1:1:2.7, and the concentration of transition metal ions is 0.2 mol L^{-1}. The mixture is stirred for 10 min, and then poured into a 50 mL Teflon vessel, the Teflon vessel then sealed in a stainless-steel autoclave. Then it is put into a furnace, and then heated at 100 °C–180 °C for different reaction time from 1 h to 24 h, and the temperatures in the autoclave are measured. After the solvothermal reaction finish, the autoclave is taken out from the furnace and then cooled down at room temperature. Apparent pH is recorded through the method of diluting supernatant 10 times with distilled water. Samples are also centrifuged, and then dried at 80 °C for 12 h. Finally, carbon coated $LiMn_{0.9}Fe_{0.1}PO_4$ is obtained by sintering of the mixture of the solvothermal product with 5 wt% carbon by sucrose at 650 °C for 5 h under argon atmosphere.

Previous reports on the solvothermal synthesis always regarded the heating temperature as reactor temperature [20–30]. However, we find that there is a significant difference between the heater temperature and the reactor temperature. Therefore, we calibrate the temperature. The details are in Supplementary data.

2.2. Characterization

The samples are characterized by powder XRD (Bruker D8 Advance X-ray diffractometer in a Bragg–Brentano configuration), SEM (JSM-5600LV, JEOL, Japan), FTIR (PerkinElmer) and TEM (FEI, Tecnai G^2 20). The pH is measured by microprocessor pH meter (pHS-25, Shanghai).

2.3. Electrochemical measurements

The electrochemical measurements are carried out by using a 2032-type coin cell. The electrolyte is 1 M $LiPF_6$ dissolved in volume ratio of 1:1:1 with ethylene carbonate/dimethyl carbonate/ethylmethyl carbonate. The electrode is prepared in mass ratio of 8:1:1 with cathode composite/acetylene black/poly (vinylidene fluoride). Galvanostatic charging–discharging tests are carried out on Land CT2001A cycler (Wuhan Kingnuo Electronic Co.) in a voltage range 2.5–4.5 V.

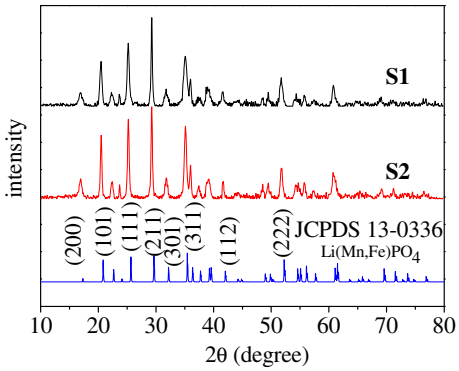

Fig. 1. X-ray diffraction (XRD) patterns of Li(Mn, Fe)PO_4.

3. Results and discussion

3.1. Sample characterization

The influence of feeding sequences for $LiFePO_4$ synthesis has already illustrated in our previous report [31]. In this study, the synthesis of $LiMn_{0.9}Fe_{0.1}PO_4$ by two feeding sequences (S1 = L + P + M, S2 = M + P + L) is investigated by solvothermal process at 180 °C for 12 h. In order to study the crystal structure of the product, powder X-ray diffraction (XRD) test is carried out. As shown in Fig. 1, all of the XRD patterns can be indexed as the orthorhombic Li(Mn, Fe)PO_4 (space group Pnmb, JCPDS Card No: 13-0336). However, as shown in Table 1, the composition of the product shows difference in Li proportion.

To confirm the horizontal face of two LMFP samples with different feeding sequences, high-resolution transmission electron microscopy (HRTEM) is applied for analysis. Figs. 2 and 3 are SEM and TEM images of samples S1 and S2.

Fig. 3 shows that the morphology of S1 = L + P + M is nanoplate and the (100) face which is perpendicular to (010) face is the exposed surface, nevertheless, the morphology of S2 = M + P + L is nanorod and the exposed surface is (010) face which is perpendicular to (100) face and (001) face. The result obtained shows that the product of S2 feeding sequence expose a large (010) face and the [010] direction is the thinnest direction of the particle.

The differences of morphology and crystal orientation are result of the effect of precursor and nuclei. The precursor of S2 is $M_3(PO_4)_2$ (M = Mn, Fe) and the precursor of S1 is Li_3PO_4. From our result we deduce that the constitution of precursor would influence synthetic process and will discuss that in detail in our further work.

Electrochemical performance tests are carried out for the $LiMn_{0.9}Fe_{0.1}PO_4$ samples of S1 and S2. Fig. 4 is the charge/discharge data of $LiMn_{0.9}Fe_{0.1}PO_4$ of two feeding sequence. The data shows that the sample S2 delivers a capacity of 130.6 mAh g^{-1} at the current density of 0.1C, which is much higher than 81.2 mAh g^{-1} of S1. From the data, we find out that the S2 has a better performance in both polarization and discharge capability. $LiMn_{0.9}Fe_{0.1}PO_4$ particles in [010] direction present the most facile pathway for lithium

Table 1
Cell parameters of different feeding sequences S1 and S2.

Feeding sequences	*a* (Å)	*b* (Å)	*c* (Å)	Volume (Å^3)
S1 = L + P + M	10.4219	6.0806	4.7519	301.14
S2 = M + P + L	10.4194	6.0827	4.7469	300.85

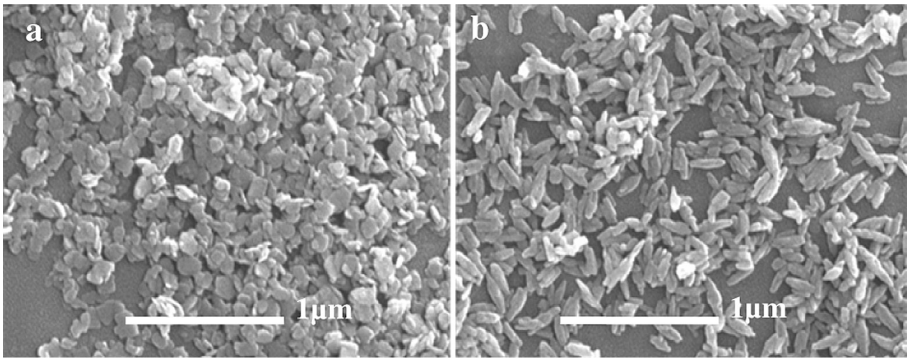

Fig. 2. Scanning electron microscopy (SEM) images of samples: (a) nanoplates LFMP obtained by S1 (L + P + M) feeding sequence; (b) nanorods LFMP obtained by S2 (M + P + L) feeding sequence.

ion, and increase the diffusion across the surface of the (010) face, so that lead to the enhancement of Li^+ ions conductivity [32].

3.2. Reaction mechanism

For solvothermal process, the phase and element composition of the mixture of different reaction time can be analyzed by XRD and ICP. The XRD patterns show that all of the samples are pure LMFP, except for the sample '0 h' whose major phase is $Mn_3(PO_4)_2$. ICP is used to analyze the content of each elements of the product. The apparent pH value of the solution is also recorded.

Figs. 5 and 6 present the change of the apparent pH and the composition of the product during the solvothermal reaction of different reaction time at 180 °C respectively. The pH value test is used to explore the reaction mechanism from the reaction environment. Our data shows that the pH value decreases at the initial 2 h and increases rapidly to 5.56 at 4 h, then the pH value decreases again until 12 h. After 12 h, pH value increases slightly and then stops at a constant value of about 3.5.

The reaction can be expressed by a five-step process: (a) at the beginning, $M_3(PO_4)_2$ (M = Fe, Mn) is instantly obtained by reaction of $MnCl_2$ (or $FeSO_4$) with H_3PO_4 (Eq. (1)) for the feeding sequence

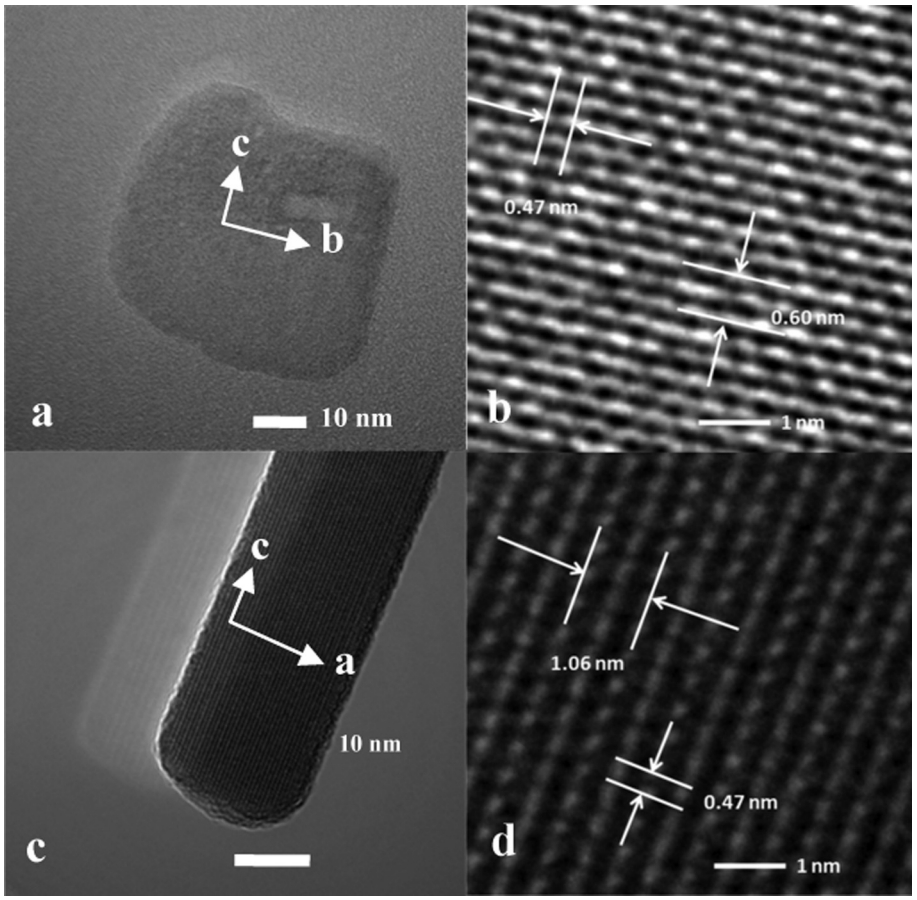

Fig. 3. HRTEM images of samples: (a) LFMP nanoplate obtained by S1 (L + P + M) feeding sequence; (c) LFMP nanorod obtained by S2 (L + P + M) feeding sequence. HRTEM magnified images of samples: (b) obtained by S1 (L + P + M) feeding sequence; (d) obtained by S2 (L + P + M) feeding sequence.

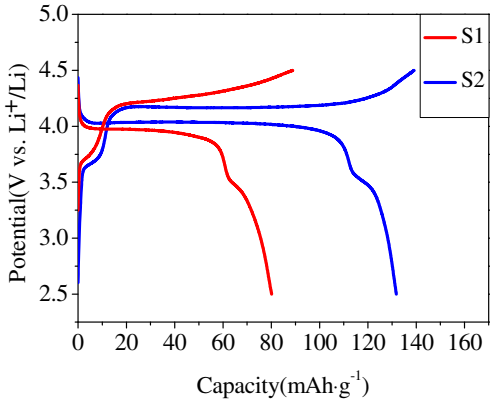

Fig. 4. Charge–discharge galvanostatic curves of samples: S1 obtained by feeding sequence L + P + M; S2 obtained by feeding sequence M + P + L.

M + P + L; (b) LMFP is synthesized by reaction of $M_3(PO_4)_2$ and LiOH at the initial 2 h (Eq. (2)), in the light of the product element proportion of Li and M increasing, and pH decreasing; (c) remnant H_3PO_4 participated in the reaction at this stage (Eq. (3)).; (d) at reaction time from 4 h to 12 h, the element proportion of N_{Li}/N_p of the product continued to increase, and the pH value keep decrease, this indicated that excess LiOH would participate in reaction; (e) after 12 h later, the M content of product dissolved out from product, the pH value maintain 3.5 (Eq. (4)).

$$MCl_2(aq) + H_3PO_4(aq) \leftrightarrow 1/3M_3(PO_4)_2(aq) + 1/3H_3PO_4(aq) + 2HCl(aq) \quad (1)$$

$$M_3(PO_4)_2(aq) + 2LiOH(aq) \leftrightarrow 2LiMPO_4(s) + M(OH)_2(s) \quad (2)$$

$$M(OH)_2(s) + H_3PO_4(aq) + LiOH(aq) \leftrightarrow LiMPO_4(s) + 3H_2O \quad (3)$$

$$M^{2+} + 2H_2O \leftrightarrow M(OH)_2(s) + 2H^+ \quad (4)$$

From above analysis, we can draw a conclusion that 4 h is sufficient for the reaction because of the pH value rebounding. We can also infer that $V_{LMP} > V_{LFP}$ in the whole synthesis speeding for the content of Mn/Fe are larger than 0.9.

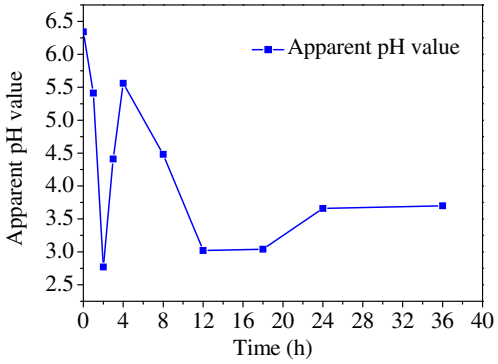

Fig. 5. The curve of solvent apparent pH changing with reaction time.

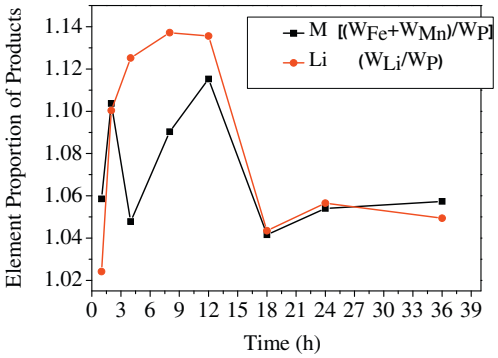

Fig. 6. The element proportion of product (relative to 100% P).

3.3. The influence of the reaction temperature and time

3.3.1. Ambient temperature variation influence

The temperature of the solvothermal reaction is also investigated to identify its influence on electrochemical performance, while keeping the reaction time at 12 h. All samples are collected after solvothermal temperature at 100 °C, 120 °C, 150 °C, 180 °C. The XRD data show that all of the samples obtained are pure phases LMFP. Fig. 7 shows the SEM image of LMFP after different solvothermal reaction temperatures. SEM data shows that the morphology of LMFP would turn more regular with the reaction temperature increases from 100 °C to 180 °C.

All of the samples are sintered with 5 wt% carbon by sucrose at 650 °C for 5 h under argon protection with a heating rate of 5 °C min^{-1}. Fig. 8 is the data of the first charge–discharge cycle at a current density of 14 mA g^{-1} for all of the carbon coated LMFP products. The capacity of the products increases with increases of temperature. Therefore, ambient temperature variation could directly affect morphology and size, leading to variation in capacity.

3.3.2. Reaction time variation influence

Reaction time of the solvothermal reaction is also investigated with the reaction temperature keep at 180 °C. Samples are collected after solvothermal treatment for 1 h, 2 h, 4 h, 8 h, 12 h, 18 h, and 24 h. The XRD patterns show that all of the samples are pure phases. The SEM images show that there are no obvious changes in morphology after 4 h of reaction. Fig. 9 shows the image of nanorod LMFP after 4 h of solvothermal reaction and the average size of the particles is 250 nm.

Fig. 10 shows the data of the first charge–discharge cycle at current density of 14 mA g^{-1} for all of the carbon coated LMFP products. Our data reveals that the discharge capacity of the samples increases when reaction time is less than 4 h and decreases with the reaction time from 4 h to 24 h, which means that 4 h is the optimum reaction time. Therefore, increasing reaction time affect less on morphology; on the contrary, the longer of the reaction time will be adverse to capacity improve.

3.3.3. The influence of defects in EG-medicated LMFP particles

The point defect concentration plays an important role on Li^+ ion migration. Defects of M_{Li} (M = Fe, Mn), which Li sites are occupied by divalent M ions, would easily form in $LiMPO_4$ [33,34] crystal. Chung et al. have directly observed such defects under the high-angle annular dark-field scanning TEM [35]. FTIR is used to get the detail crystal structural information. Different reaction temperature and time are performed to figure out a relation between antisite defects and the absorption band. The absorption band around 1000 cm^{-1}, which is symmetric stretching P–O

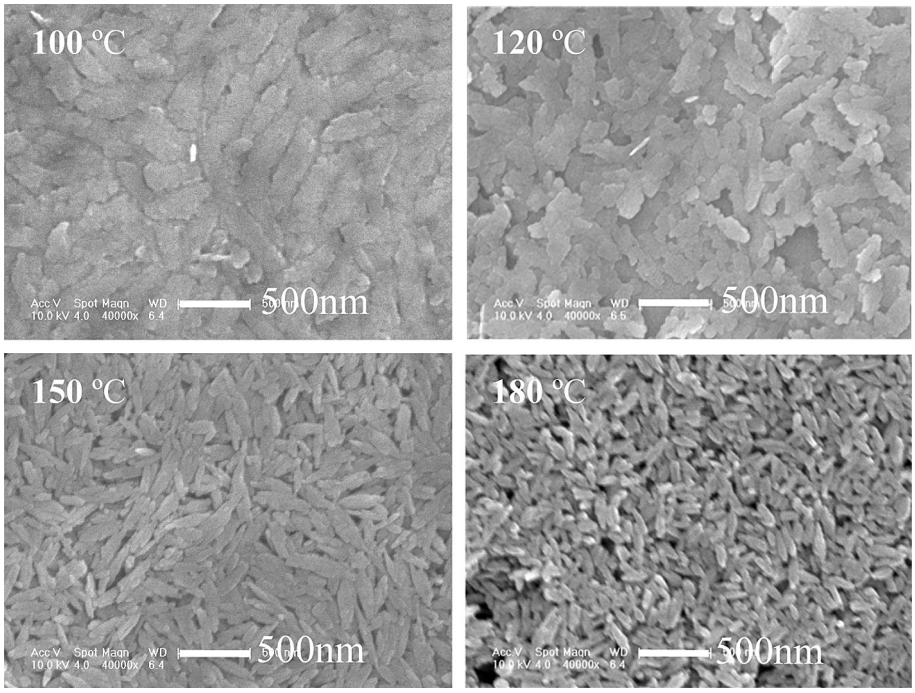

Fig. 7. The SEM images of LFMP after solvothermal treatment for 12 h at different solvothermal reaction temperature.

vibration (v_1), and it is very sensitive to the lithium and iron ions that surrounded by PO_4 tetrahedral [36–38]. Fig. 11 shows the FTIR spectra of the samples at various temperature and time, respectively. In order to observe the movement of the peak, a striking red box is added.

We speculated that defects M_{Li} are just like N-semiconductor, which can provide more negative electron carriers. The more M mixed, the higher free electron concentration, leading to better conductivity. Because ambient temperature samples are all treated for 12 h, defects M_{Li} would exist less; this is the reason why defect concentration of the M_{Li} is susceptible to the reaction time, rather than temperature.

To understand the interesting shift around P–O vibration (v_1) peak, we added one chemically delithiated ($M = Mn_{0.9}Fe_{0.1}$) infrared absorption curve. After 36 h 180 °C solvothermal synthesis LMFP and 36 h delithium in an Ar-filled glove box, the content of Li (relative to 100% content M) decreased to $x = 0.03$. This delithiated product is regard as near defect-free for less lithium could obstruct ion migration. The P–O vibration (v_1) peak of near defect-free Li_xMPO_4 ($x = 0.03$) is located at 939.3 cm^{-1}, but for the sample of 4 h $Li_{1.13}Mn_{0.95}Fe_{0.10}PO_4$ it locates at 1000.0 cm^{-1} so that it is away from the near defect-free LMFP v_1 peak. It is reasonable to conclude that the v_1 peak shift left may represent the increase defects concentration of M_{Li} antisite.

From above discussion, we can draw the conclusion that the larger P–O vibration (v_1) peak value means the more defects concentration of M_{Li} antisite; and represents higher content of Li (Fig. 6 Li relative to 100% content M). As shown in the charge–discharge data of Fig. 10, defects M_{Li} could improve the electrochemical performance.

3.4. Electrochemical rate performance

Fig. 12 shows the rate performance of the carbon coated LMFP materials that obtained at 4 h of solvothermal reaction. The discharge data of $LiMn_{0.9}Fe_{0.1}PO_4$/C composite nanorod at different discharge current in the first cycle are presented in Fig. 12a). At 0.1C,

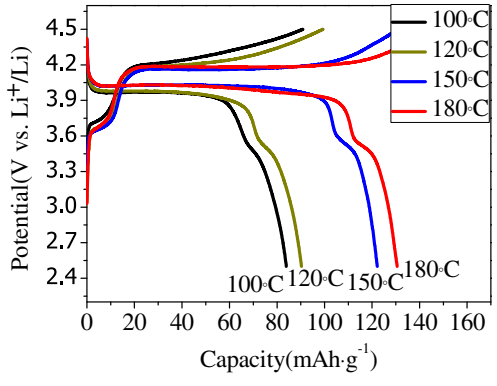

Fig. 8. Comparison of the charge–discharge galvanostatic curves of the carbon coated LMFP: solvothermal treatment for 12 h at different solvothermal reaction temperature.

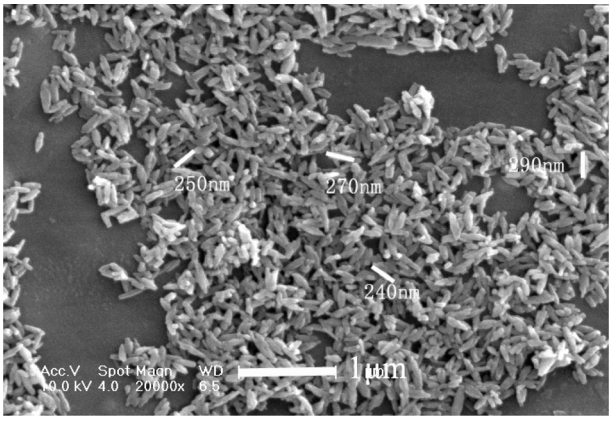

Fig. 9. The image of nanorod LMFP after 4 h solvothermal reaction time under 180 °C.

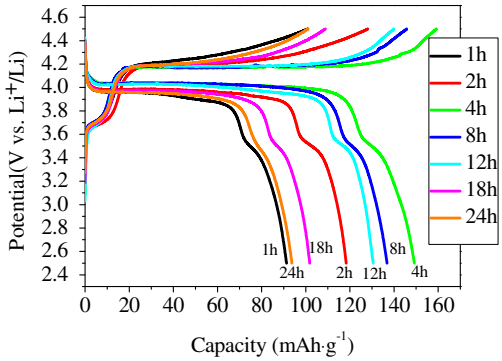

Fig. 10. Comparison of the charge–discharge galvanostatic curves of the carbon coated LFMP: solvothermal treatment with different solvothermal reaction time under 180 °C.

the $LiMn_{0.9}Fe_{0.1}PO_4/C$ delivers a discharge capacity of 149 mAh g^{-1}. It delivers discharge capacities of 138.0, 129.3, 124.1, 116.4 mAh g^{-1} at 0.2C, 0.5C, 1C, 2C, respectively. Upon increasing the current rate, the $LiMn_{0.9}Fe_{0.1}PO_4/C$ composites show an obvious reduced storage capacity due to increasing of the polarization [39]. Fig. 12b) shows the rate and cycle performances. It is found that the cell capacity can recover to its original value and this indicates that the cathode has a stable formation after high rate cycles.

4. Conclusions

In summary, the feeding sequence plays an important role for solvothermal synthesis of nano-LMFP materials. Our result shows that the $LiMn_{0.9}Fe_{0.1}PO_4$ obtained from M + P + L feeding sequence has nanorod shape and (010) orientation and also has high electrochemical performance. A reaction mechanism of "five-step process" for M + P + L feeding sequence is proposed. For $LiMn_{0.9}Fe_{0.1}PO_4$, the morphology and size of the particles be affected by reaction temperature, and the electrochemical capacity is affected by reaction time. From infrared absorption, we conclude that large value of P–O vibration (ν_1) peak indicates more defects of M_{Li}, and that leads to better electrochemical performance.

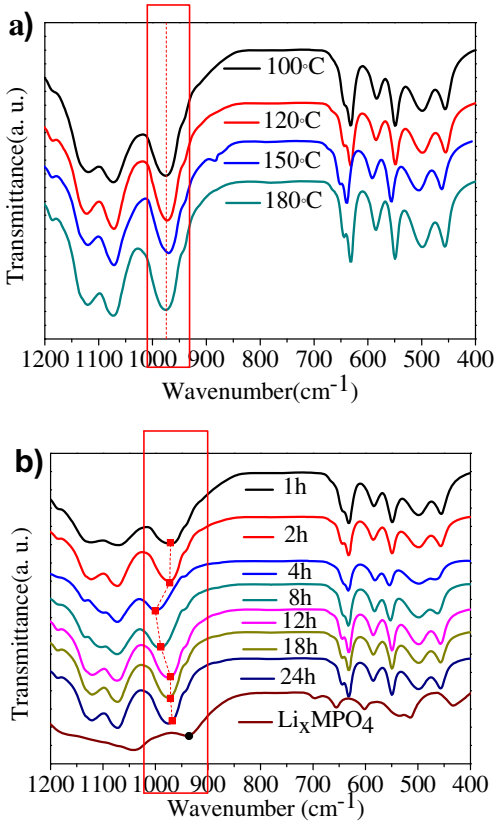

Fig. 11. The FTIR spectra of the samples at a) various reaction temperature and b) reaction time.

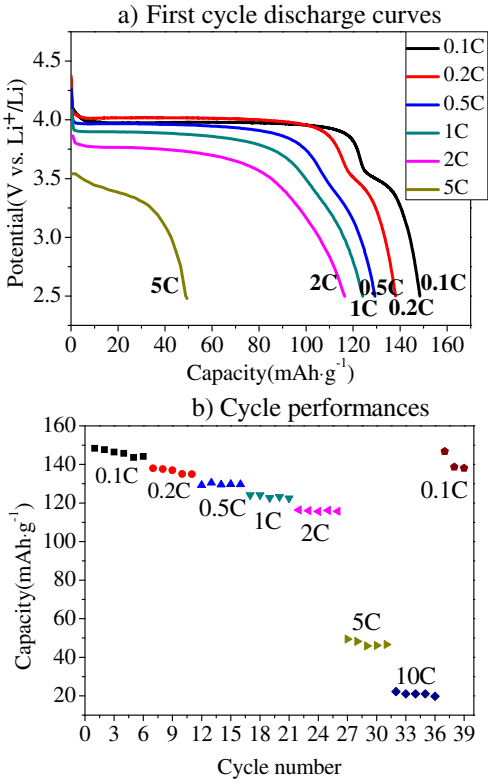

Fig. 12. $LiMn_{0.9}Fe_{0.1}PO_4/C$ composite electrochemical performance of a) the first cycle discharge curves of at different current rates b) the rate and cycle performances.

Acknowledgments

This work is supported by the MOST (Grant No. 2011CB935902, No. 2013CB934000, No. 2010DFA72760, No. 2011CB711202, No. 2013AA050903, No. 2011AA11A257 and No. 2011AA11A254), the China Postdoctoral Science Foundation (Grant No. 2013M530599 and No. 2013M540929), the Tsinghua University Initiative Scientific Research Program (Grant No. 2010THZ08116, No. 2011THZ08139, No. 2011THZ01004 and No. 2012THZ08129) and State Key Laboratory of Automotive Safety and Energy (Grant No. ZZ2012-011).

Appendix A. Supplementary data

Supplementary data related to this article can be found at http://dx.doi.org/10.1016/j.jpowsour.2013.12.010.

References

[1] A.K. Padhi, K.S. Nanjundaswamy, J.B. Goodenough, J. Electrochem. Soc. 144 (1997) 1188–1194.
[2] M. Higuchi, K. Katayama, Y. Azuma, M. Yukawa, M. Suhara, J. Power Sources 119 (2003) 258–261.
[3] L. Yuan, Z. Wang, W. Zhang, X. Hu, J. Chen, Y. Huang, J.B. Goodenough, Energy Environ. Sci. 4 (2011) 269–284.
[4] C. Nan, J. Lu, C. Chen, Q. Peng, Y. Li, J. Mater. Chem. 27 (2011) 9994–9996.

[5] D. Wang, H. Buqa, M. Crouzet, G. Deghenghi, T. Drezen, I. Exnar, N.H. Kwon, J.H. Miners, L. Poletto, M. Gratzel, J. Power Sources 189 (2009) 624–628.
[6] T.H. Kim, H.S. Park, M.H. Lee, S.Y. Lee, H.K. Song, J. Power Sources 210 (2012) 1–6.
[7] S. Ju, H. Peng, G. Li, K. Chen, Mater. Lett. 74 (2012) 22–25.
[8] H.K. Song, K.T. Lee, M.G. Kim, L.F. Nazar, J. Cho, Adv. Funct. Mater. 20 (2010) 3818–3834.
[9] C. Delacourt, L. Laffont, R. Bouchet, C. Wurm, J.B. Leriche, M. Morcrette, J.M. Tarascon, C. Masquelier, J. Electrochem. Soc. 152 (2005) A913–A921.
[10] S.K. Martha, B. Markovsky, J. Grinblat, J. Electrochem. Soc. 156 (7) (2009) A541–A552.
[11] V. Aravindan, J. Gnanaraj, Y.S. Lee, S. Madhavi, J. Mater. Chem. A 1 (2013) 3518–3539.
[12] N.N. Bramnik, H. Ehrenberg, J. Alloys Compd. 464 (2008) 259–264.
[13] N.N. Bramnik, K. Nikolowski, C. Baehtz, K.G. Bramnik, H. Ehrenberg, Chem. Mater. 19 (2007) 908–915.
[14] D. Choi, D. Wang, I.T. Bae, J. Xiao, Z. Nie, W. Wang, V.V. Viswanathan, Y.J. Lee, J.G. Zhang, G.L. Graff, Z. Yang, J. Liu, Nano Lett. 10 (2010) 2799–2805.
[15] N.H. Kwon, T. Drezen, I. Exnar, I. Teerlinck, M. Isono, M. Graetzel, Electrochem. Solid State Lett. 9 (2006) A277–A280.
[16] G. Amold, J. Garche, R. Hemmer, J. Power Sources 119 (2003) 247–251.
[17] T. Li, T. Mei, Y.C. Zhu, H.X. Huang, Y.T. Qian, Chem. Lett. 40 (2011) 837–839.
[18] Y. Wang, Y. Yang, Y. Yang, Y. Yang, H. Shao, Mater. Res. Bull. 44 (2009) 2139–2142.
[19] M. Jo, H.C. Yoo, Y.S. Jung, J. Cho, J. Power Sources 216 (2012) 162–168.
[20] J.J. Chen, S.J. Wang, M.S. Whittingham, J. Power Sources 174 (2007) 442–448.
[21] S. Yang, P.Y. Zavalij, M.S. Whittingham, Electrochem. Commun. 3 (2001) 505–508.
[22] J.J. Chen, S.J. Wang, M.S. Whittingham, Electrochem. Commun. 8 (2006) 855–858.
[23] K. Dokko, S. Koizumi, K. Sharaishi, K. Kanamur, J. Power Sources 165 (2007) 656–659.
[24] J.F. Qian, M. Zhou, Y.L. Cao, X.P. Ai, H.X. Yang, J. Phys. Chem. C 114 (2010) 3477–3482.
[25] K. Dokko, S. Koizumi, K. Kanamura, Chem. Lett. 35 (2006) 338.
[26] J.J. Chen, M.J. Vacchio, S.J. Wang, N. Chernova, P.Y. Zavalij, M.S. Whittingham, Solid State Ionics 178 (2008) 1676–1693.
[27] K. Shiraishi, K. Dokko, K. Kanamura, J. Power Sources 146 (2005) 555–558.
[28] C.A.J. Fisher, M.S. Islam, J. Mater. Chem. 18 (2008) 1209–1215.
[29] N. Recham, M. Armand, L. Laffont, J.M. Tarascon, Electrochem. Solid State Lett. 12 (2009) A39–A44.
[30] B. Ellis, W.H. Kan, W.R.M. Makahnouk, L.F. Nazar, J. Mater. Chem. 17 (2007) 3248–3254.
[31] L. Wang, X. He, W. Sun, J. Wang, Y. Li, S. Fan, Nano Lett. 12 (2012) 5632–5636.
[32] R. Amin, P. Balaya, J. Maier, Electrochem. Solid State Lett. 10 (2007) A13–A16.
[33] R. Malik, D. Burch, M. Bazant, G. Ceder, Nano Lett. 10 (2010) 4123–4127.
[34] P. Axmann, C. Stinner, M. Wohlfahrt-Mehrens, A. Mauger, F. Gendron, C.M. Julien, Chem. Mater. 21 (2009) 1636–1644.
[35] S.Y. Chung, Y.M. Kim, S.Y. Choi, Adv. Funct. Mater. 20 (2010) 4219–4232.
[36] V. Koleva, R. Stoyanova, E. Zhecheva, Mater. Chem. Phys. 121 (2010) 370–377.
[37] A. Ait Salah, P. Jozwiak, K. Zaghib, J. Garbarczyk, F. Gendron, A. Mauger, C.M. Julien, Spectrochim. Acta Part A Mol. Biomol. Spectrosc. 65 (2006) 1007–1013.
[38] D. Lepage, C. Michot, G. Liang, M. Gauthier, S. Schougaard, Angew. Chem. Int. Ed. 50 (2011) 6884–6887.
[39] X. Wu, L. Jiang, F. Cao, Y. Guo, L. Wan, Adv. Mater. 21 (2009) 2710–2714.